T. Methling, M. Braun-Unkhoff, U. Riedel, A novel linear transformation model for the analysis and optimisation of chemical kinetics, Combustion Theory and Modelling 21(3) (2017) 503–528.

The original publication is available at www.informaworld.com

http://dx.doi.org/10.1080/13647830.2016.1251616

Or use open URL link
http://www.informaworld.com/openurl?genre=article&issn=1364-7830&volume=21&issue=3&spage=503;

Combustion Theory and Modelling
Vol. 00, No. 00, Month 200x, 1–39

RESEARCH ARTICLE

A novel linear transformation model for the analysis and optimisation of chemical kinetics

Torsten Methling*, Marina Braun-Unkhoff and Uwe Riedel

German Aerospace Center (DLR), Institute of Combustion Technology, Stuttgart, Germany

(*Received 00 Month 200x; final version received 00 Month 200x*)

In this study a novel model for the analysis and optimisation of numerical and experimental chemical kinetics is developed. Concentration time profiles of non-diffusive chemical kinetic processes and flame speed profiles of fuel oxidiser mixtures can be described by certain characteristic points, so that relations between the coordinates of these points and input parameters of chemical kinetic models become almost linear. This linear transformation model simplifies the analysis of chemical kinetic models, hence creating a robust global sensitivity analysis and allowing a quick optimisation and reduction of these models. Firstly, in this study the model is extensively validated by the optimisation of a syngas combustion model with a large data set of imitated ignition experiments. The optimisation with the linear transformation model is quick and accurate, revealing the potential to decrease numerical costs of the optimisation process by at least one order of magnitude, compared to established methods. Additionally, the optimisation on this data set demonstrates the capability of predicting reaction rate coefficients, more accurately than by currently known confidence intervals. In a first application, methane combustion models are optimised with a small experimental set, consisting of OH(A) and CH(A) concentration profiles from shock tube ignition experiments, species profiles from flow reactor experiments and laminar flame speeds. With the optimised models, especially the predictability for the flame speeds of mixtures of hydrogen, carbon monoxide and methane can be increased compared to established models. With the analysis of the optimised models, new information for the low pressure reaction coefficient of the fall-off reaction H+CH_3(+M)<=>CH_4(+M) is determined. In addition, the optimised combustion model is quickly and efficiently reduced to validate a new rapid reduction scheme for chemical kinetic models.

Keywords: chemical kinetics; analysis; optimisation; reduction; biogenic gas

Nomenclature

Latin

A	matrix with brute force sensitivities
A	pre-exponential factor of Arrhenius equation (variable)
b	temperature exponent of Arrhenius equation
c	concentration (mol m^{-3})
D	number of characteristic points
d	distance between characteristic points
E_A	activation energy of Arrhenius equation (J mol^{-1})
F	fitness of chemical kinetic model
k	rate coefficient (variable)

*Corresponding author. Email: torsten.methling@dlr.de

ISSN: 1364-7830 print/ISSN 1741-3559 online

DOI: 10.1080/1364783YYxxxxxxx
http://www.tandfonline.com

k_{low}	fall-off rate coefficient of low pressure regime (variable)
P	number of normalised parameters
p	pressure (Pa)
R	ideal gas constant ($\mathrm{J\,mol^{-1}\,K^{-1}}$)
S	global sensitivity
$S_{r,j}$	sensitivity of characteristic point j on reaction r
T	temperature (K)
t	time (s)
u_{l}	laminar burning velocity ($\mathrm{m\ s^{-1}}$)
u_{l}^{0}	laminar flame speed ($\mathrm{m\ s^{-1}}$)

Greek

α	relaxation factor
β	concentration ratio in relation to the maximum
Γ	characteristic point for laminar flame speeds
γ	concentration ratio in relation to the maximum
Π	characteristic point for concentration profiles
σ	standard deviation
τ	normalised parameter
φ	equivalence ratio

Subscripts

c	concentration related
e	direction indicator meaning from maximum to end
i	normalised parameter number
j	characteristic point number
m	numbering index
max	maximum
n	iteration number
r	reaction number
rms	root mean square
s	direction indicator meaning from start to maximum
t	time related
u	laminar flame speed related
β	concentration ratio in relation to the maximum
Θ	original value
φ	equivalence ratio related
0	base value
$-$	lower boundary of a parameter
$+$	upper boundary of a parameter

1. Introduction

With an intensified focus on sustainability and environmental awareness of society and economy, new synthetic and biogenic fuels emerge into markets. Regarding energy demands, combustion applications offer flexible operations and have high energy and power densities, thus being broadly irreplaceable for electricity, heat and transportation. In this context, combustion applications need to be adapted or newly designed to assure reliable operation at low emission levels with the new

fuels of interest. Consequently, accurate and efficient chemical kinetic models, implementable in computational fluid dynamics (CFD), are needed for a sophisticated design of combustion applications. But, even seemingly simple chemical kinetic models for synthetic or biogenic fuels, like syngas or methane, have high parameter uncertainties and partially, do not accurately reproduce results of fundamental experiments (see e.g. [1–3]).

To investigate the reasons for disagreements between simulations and experiments, it is of vast importance to identify and accurately determine important parameters—mainly rate coefficients and their parameters—of chemical kinetic models for the combustion process of interest. Thereby, numerical investigations of these parameters can be numerically expensive because, for the simulation of combustion processes, non-linear ordinary differential equation (ODE) systems must be solved, that often appear to be stiff due to different scales of rate coefficients.

For the identification of important model parameters, well established methods of local or global sensitivity analysis [4–6] can be utilised. Whereas local sensitivity analysis is numerically cheap, but limited to parameter sensitivity information at local coordinates (space and time) of the simulation, global sensitivity analysis gives more comprehensive information on parameter sensitivity of the combustion system, but is numerically expensive, due to hypercubic spaces spanned by a high number of model parameters. Once the important parameters or rate coefficients respectively are identified, they need to be determined with high accuracy. Parameters of chemical kinetic models are often estimated by quantum chemical simulations (e.g. [7]) or by direct experimental measurements (e.g. [8]). More recently the estimation of parameters by optimisation on more complex combustion experiments than direct measurements is focused on by many researchers [9–11]. Examples for these so called indirect experiments are measurements of ignition delay times or species profiles in shock tube, rapid compression machine or flow reactor experiments of complex simultaneous chemical kinetics. Thereby, the optimisation on a large data set of these experiments is very challenging because of the limited analysis of non-linear and mostly stiff ODE with the solution being numerical expensive. Current approaches for the optimisation are methods based on genetic algorithms (e.g. [12]) or methods based on response surface approximation (e.g. [11]). Both methods have been successfully applied to optimisation of chemical kinetic models before, but are computational expensive (see Section 3).

Therefore, the objective of this work is the optimisation of a chemical kinetic model for the combustion of biogenic gas mixtures, to reproduce experimental results more accurately, thus, increasing the prediction capability of CFD simulations for numerical design of combustion application. The target data for the optimisation are laminar flame speed profiles [13] and concentration profiles of exited OH(A) and CH(A) radicals gained from shock tube ignition experiments of methane oxygen mixtures [14]. Further target data are species profiles from flow reactor experiments of methane combustion [15]. By the utilisation of the whole concentration profiles, more information on the time scales of the production and consumption of intermediates is gained. This benefits the quality of the optimised models, but is also more challenging for the optimisation problem with the underlying non-linear stiff ODE. To reduce the numerical effort of the optimisation, the optimisation problem was transformed, and the new linear transformation model (linTM) was created. With the linTM the relation between input or model parameters and output parameters or species profiles or laminar flame speed profiles is linearised and at the same time keeping a high accuracy compared to the non-linearised system. This new method reveals the potential of reducing numerical costs of optimisation problems by at least one order of magnitude. The investigation in this work shows

that the linTM surpasses the capability of only optimising chemical kinetics. With the linTM it is also possible to create a new robust and quantitative global sensitivity coefficient of reactions for experimental data sets, which is numerically cheap compared to established global sensitivity analysis methods. The combination of the quantitative sensitivity analysis and efficient optimisation allows a new rapid and efficient reduction of chemical kinetic models, which serves as a new reduction tool besides established tools like reaction flow analysis or lumping of chemical kinetic models (e.g. [16, 17]).

2. Modelling

In this study, we develop the linear transformation model (linTM) for the analysis and optimisation of chemical kinetic processes. The linTM changes or transforms the definition of input parameters of the chemical kinetic model and the output parameters of numerical simulations or experiments. This transformation allows new methods for analysis, optimisation and reduction of chemical kinetic models. For the investigation on parameter behaviour within this work, the simulations were performed with the open-source software Cantera [18] and pre- and post-processing routines were created in the programming language python.

2.1 *The fundamentals of the linear transformation model*

Important steps of the linTM are the definitions of the input parameters of chemical kinetic models and output parameters of chemical kinetic processes, such as species profiles from combustion processes or laminar flame speed profiles. The objective of the linTM is to simplify the relation between these input and output parameters by linearisation, and at the same time keeping a high accuracy describing the relation between these parameters.

2.1.1 Definition of input parameters

Exceedingly important input parameters of the chemical kinetic model are the rate coefficients k. A rate coefficient k_r of a reaction r is mostly given by the extended Arrhenius equation:

$$k_r(T) = A_r T^{b_r} \exp\left(-E_{\mathrm{A},r}/(RT)\right), \tag{1}$$

for which A is the pre-exponential factor, b is the temperature exponent and E_A is the activation energy. The rate coefficient k and its uncertainty are usually estimated by measurements or calculations at certain temperatures or within temperature ranges. These constraints on k mathematically cause the constraints or boundaries of each Arrhenius parameter A, b or E_A to be dependent on the other two remaining parameters, making the direct use of these parameter as input parameters more complex (see e.g. [10, 11]). Due to that, in the linTM the Arrhenius parameter A, b and E_A are not directly used as input parameters. The input parameters of the linTM are shifts of the rate coefficient k at certain user defined temperatures T_1, T_2 and T_3. As shown in Figure 1 the shifts are given by logarithmic differences to the base rate coefficient k_0:

$$\Delta \ln(k_r(T_{r,m})) = \ln\left(k_r(T_{r,m})/k_{r,0}(T_{r,m})\right) \qquad m = 1, 2, 3. \tag{2}$$

With these three shifts in Equation (2) a new set of Arrhenius parameters can be determined (method *k3*). By using the shifts as input parameters, analysis and optimisation become simplified because the constraints of the parameters are well defined and more decoupled.

For reactions with large uncertainty bands of k, using method *k3* might cause E_A to become physically unlikely (e.g. negative). For these reactions and/or for well known constraints of E_A, E_A or the distance ΔE_A to the value of the base model can be used a an input parameter directly. Similar to method *k3* and Equation (2), the remaining parameters A and b can then be determined with two shifts of k at the user defined temperatures T_1 and T_2 (method *Ekk*).

For a simplification, all the different input parameters of the chemical kinetic model are normalised by their maximum value, to form the normalised parameter τ_i, as shown in Figure 1. The index i is the numbering index for all input parameters of the model and this notation is kept throughout this paper.

2.1.2 Relation between input parameters and species profiles of homogeneous combustion processes

Optimisation of species profiles is complicated because the relation between concentrations c as a function of time t and input parameters of chemical kinetic models are not necessarily monotonous [19]. This causes the optimisation problem having additional local minima, resulting in the need of using e.g. genetic algorithms as an optimisation approach [19, 20]. The major point of the linTM is to change the description of concentration time profiles. Instead of looking at concentration c as a function of time t, the linear transformation model rather looks at time being a function of the concentration. Since times cannot be uniquely defined by concentrations, we define characteristic points $\Pi_{j,\beta,\mathrm{s/e}}(t_j|c_j = \beta c_{j,\max})$ on the concentration time profile by means of relative maximum concentration and direction of the process (see Figure 2). The subscript j is a numbering index for the characteristic points. β is the relative concentration in relation to the maximum concentration. The letter subscript indicates the direction, at which s means directing from start to maximum and e means directing from maximum to end. The letter subscript is omitted for $\beta = 100\%$. This is also adaptable for concentration time profiles with several local maxima, for which an additional indicator for the certain maximum is needed, e.g. numbering by chronological order. Similar to the input parameters, the numbering index j is kept throughout this complete manuscript.

The investigation of the influence of parameter τ_1 (from Figure 1) on the simulation results is shown in Figures 2 to 4. For this investigation the method *k3* was used for a rate coefficient k_1. Apart from τ_1, every parameter of the chemical kinetic model is held constant at zero, meaning they are unchanged from the base model. Figure 2 shows the calculated concentration profiles for the unchanged rate coefficient of the base model k_0 and the rate coefficients relating to the upper boundary + and the lower boundary − of τ_1. To compare and evaluate the simulation, the characteristic points of the simulation are compared to the ones of the original model 0 by logarithmic differences $d_{j,t/c}$ of the time and the concentration coordinate, definded by:

$$d_{j,t} = \ln(t_j/t_{j,0}), \tag{3a}$$

$$d_{j,c} = \ln(c_j/c_{j,0}). \tag{3b}$$

It should be noted that the distances of the concentration coordinate $d_{j,c}$ are just needed for the maximum values because the other characteristic points are dependent on the maximum values. To simplify the notation, we therefore refer to d_j as a notation for $d_{j,c}$ and/or $d_{j,t}$.

Figure 3 shows that the distances d_j are almost linear functions of τ_1. In our investigations we have seen that this linearity is valid for most model parameter τ and their corresponding confidence intervals. In Figure 4 the effect of τ_1 and τ_2 (from Figure 1) of the investigated reaction is studied, still using the method *k3*. The figure reveals a weak dependency of most gradients $\partial d_j/\partial\tau_i$ on the parameters τ_i. This is leading to the fundamentals of the linTM in Equation (4), assuming all gradients are almost constant, within their confidence intervals.

$$\frac{\partial d_j}{\partial \tau_i} \approx \text{const.} \tag{4}$$

This assumption is a strong simplification, that is not fully valid in the complete parameter domains. However, this assumption can be utilised for a robust global sensitivity analysis and optimisation with low computational costs, as shown by the validation in Section 3. The assumption in Equation (4) is also applicable for the variation method *Ekk* and other typical parametrisation of chemical kinetic models. Regarding this, the methods *k3* and *Ekk* can be similarly applied to the Arrhenius coefficients of the high and low pressure regimes of fall-off reactions. Another valid parameter would be the logarithmic difference of collision efficiencies.

2.1.3 Relation between input parameters and laminar flame speed profiles

The linTM is also applicable for laminar flame speeds u_l^0 as a function of the equivalence ratio φ. On the whole, the linear behaviour between rate coefficients and laminar flame speeds is well investigated and e.g. utilised for sensitivity analysis of laminar flame speeds (e.g. [4]). But, by the means of the linTM, the dependency of the laminar flame speed and the parameters of rate coefficients can be investigated in more detail. Similar to the characteristic points Π of the concentration time profiles, we define characteristic points $\Gamma_{j,\gamma,\mathrm{s/e}}(\varphi_j|u^0_{\mathrm{l},j} = \gamma u^0_{\mathrm{l},j,\max})$ for the laminar flame speeds. For notation of the characteristic points, γ is the ratio between the laminar flame speed of the characteristic point and the maximum flame speed. As shown in Figure 5, the changes of the laminar flame speed profiles are almost equidistant with a constant change of τ_1. Similar to the concentration time profiles, the distances $d_{j,u}$ and $d_{j,\varphi}$ are defined for the laminar flame speed profile with equations:

$$d_{j,u} = \ln(u^0_{\mathrm{l},j}/u^0_{\mathrm{l},j,0}), \tag{5a}$$

$$d_{j,\varphi} = \ln(\varphi_j/\varphi_{j,0}). \tag{5b}$$

In case the j-th characteristic point is on a laminar flame speed profile, the notation d_j refers to $d_{j,u}$ and/or $d_{j,\varphi}$.

For the analysis of these characteristic points the numerical effort is very high because a high resolution of laminar flame speeds is needed to capture all the features—e.g. maximum flame speed—of the flame speed profile. The numerical effort can be reduced because laminar flame speeds as a function of the equivalence ratio can be fitted very accurately with polynomials (see e.g. [21] for hydrogen or

[22] for natural gas). The equidistant changes in Figure 5 can also be achieved with the second order polynomial using three fitting points from the profile. For this fitting method the maximum error between predicted laminar flame speeds of the simulation—at the markers in Figure 5—and the polynomial was 1.1%. Using a third order polynomial with 4 fitting points reduced the maximum error to 0.4%. This also leads us to the conclusion that laminar flame speed profiles can be sufficiently described by 3 to 4 characteristic points. For this fitting method, it is advisable to define characteristic points with rather high relative maximum flame speeds γ because of the lower extinction levels of the laminar flame speed profiles are slower to compute and the polynomial approach has a lower quality than for the profile region around the maximum. The applicability of this approach is proven by the optimisation on flame speed profiles in the results section.

2.2 *Global sensitivity coefficient of the linear transformation model*

Even though, the linear relation between the distances d_j and parameters can also be shown for the Arrhenius parameters $\ln(A)$ and b, it is beneficial to use the variation methods *k3* and *Ekk* of Section 2.1.1. For instance, the domain boundaries of $\ln(A)$ are functions of b and E_A. The variation methods *k3* and *Ekk* use input parameters with more decoupled domains and well defined boundaries. This allows the definition of a new global sensitivity coefficient S_r for a reaction r and a set of D characteristic points for various target values on concentration or flame speed profiles. S_r is calculated by parameters τ_m to τ_{m+P_r-1}, which account for the parameters belonging to a reaction r, for which P_r is its number of parameters. The idea of this sensitivity coefficient is to find a certain parameter vector $\boldsymbol{\tau}_r$, which is defined by:

$$\boldsymbol{\tau}_r = \begin{pmatrix} \tau_m \\ \tau_{m+1} \\ \vdots \\ \tau_{m+P_r-1} \end{pmatrix} \tag{6}$$

and

$$|\boldsymbol{\tau}_r| = 1, \tag{7}$$

with the highest slope for a certain d_j defined by:

$$d_j = \sum_{i=m}^{m+P_r-1} \frac{\partial d_j}{\partial \tau_i} \tau_i. \tag{8}$$

The highest slope quantifies the change of the characteristic points' distances by the input parameters of each reaction r, and therefore is a very suitable sensitivity. Assuming an ideal linear system of independent, normalised parameters τ_i, the analytical solution for the highest slope or the specific sensitivity of the characteristic point $S_{r,j}$ respectively, is the Euclidean sum of squares:

$$S_{r,j} = \left(\sum_{i=m}^{m+P_r-1} \left(\frac{\partial d_j}{\partial \tau_i} \right)^2 \right)^{0.5}. \tag{9}$$

The gradients $\partial d_j/\partial\tau_i$ can be calculated by brute force sensitivity analysis. The global sensitivity coefficient S_r is then created by the sum of sensitivities of the characteristic points:

$$S_r = \sum_{j=1}^{D} S_{r,j}. \tag{10}$$

The weak dependency of most gradients $\partial d_j/\partial\tau_i$ on the parameters τ_i, as shown in Figure 4, leads to a very robust and quantitative sensitivity coefficient for a single reaction, which is demonstrated in more detail in Section 3.2.

2.3 *Optimisation with the linear transformation model*

The linearity of the linTM can be utilised for a simple and quick optimisation method for chemical kinetic models. The objective of the optimisation is to minimise the distances d_j in equations (3) and (5) between predictions of a chemical kinetic model and target data of characteristic points Π on species profiles and Γ on flame speed profiles. Since the gradients $\partial d_j/\partial\tau_i$ are not perfectly linear and not exactly independent on the input parameters τ_i, the optimisation needs to be solved by iterations n, starting with a base chemical kinetic model $n = 0$. To evaluate a chemical kinetic model, the fitness F for D characteristic points is formed by the sum of the absolute distances d_j:

$$F_n = \sum_{j=1}^{D} |d_{j,n}|\,. \tag{11}$$

Thus, the optimisation objective is to minimise F. With the initial base chemical kinetic model, the initial distances $d_{j,0}$ of D characteristic points can be determined, defining the distance vector $\boldsymbol{d}$, and initial gradients $\partial d_{j,0}/\partial\tau_i$ for P input parameters can be calculated, defining the matrix $\mathbf{A}$. With equations:

$$\underbrace{\begin{pmatrix} \frac{\partial d_{1,n}}{\partial\tau_1} & \frac{\partial d_{1,n}}{\partial\tau_2} & \cdots & \frac{\partial d_{1,n}}{\partial\tau_P} \\ \frac{\partial d_{2,n}}{\partial\tau_1} & \frac{\partial d_{2,n}}{\partial\tau_2} & \cdots & \frac{\partial d_{2,n}}{\partial\tau_P} \\ \vdots & \vdots & \ddots & \vdots \\ \frac{\partial d_{D,n}}{\partial\tau_1} & \frac{\partial d_{D,n}}{\partial\tau_2} & \cdots & \frac{\partial d_{D,n}}{\partial\tau_P} \end{pmatrix}}_{\mathbf{A}_n} \underbrace{\begin{pmatrix} \Delta\tau_{1,n} \\ \Delta\tau_{2,n} \\ \vdots \\ \Delta\tau_{P,n} \end{pmatrix}}_{\Delta\boldsymbol{\tau}_n} + \underbrace{\begin{pmatrix} d_{1,n} \\ d_{2,n} \\ \vdots \\ d_{D,n} \end{pmatrix}}_{\boldsymbol{d}_n} = 0 \tag{12}$$

and

$$\boldsymbol{\tau}_{n+1} = \boldsymbol{\tau}_n + \alpha\Delta\boldsymbol{\tau}_n \qquad \{\alpha \in \mathbb{R} | 0 < \alpha \leq 1\}, \tag{13}$$

a solution for the parameter vector $\boldsymbol{\tau}$, consisting of all input parameters τ_i, can be found iteratively. Taking the linear relation between distances and the input parameters into account, Equation (12) can be solved with the method of least squares (LS). Finding a solution for $\Delta\boldsymbol{\tau}_n$ might cause a parameter $\tau_{i,n+1}$ to be out of its confidence interval. To avoid this, the relaxation factor α can be set to small values, slowing down the optimisation. Instead, for a better convergence of F_{n+1}, it is beneficial to reduce the matrix $\mathbf{A}_n$ by the column of this parameter τ_i and the vector $\Delta\boldsymbol{\tau}_n$ by this τ_i and recalculate the new, reduced $\Delta\boldsymbol{\tau}_n$ and new $\boldsymbol{\tau}_{n+1}$

with Equations (12) and (13). Following this approach, α can be kept high and the optimisation converges faster.

2.4 *Rapid reduction with the linear transformation model*

The newly defined global sensitivity S_r (Section 2.2) robustly quantifies the influence of input parameters of reaction r on the output parameters of concentration or flame speed profiles (characteristic points). This relation coupled with the efficient optimisation method can be utilised with a rapid reduction scheme for chemical kinetic models:

(1) Calculate different concentration or flame speed profiles for different temperatures T, pressures p and equivalence ratios φ, representing analysis and target data for reduction and optimisation.
(2) Set all model input parameters τ_i with equal or comparable upper and lower boundaries.
(3) Calculate the global sensitivities S_r and reduce the mechanism by eliminating reactions with low S_r. This can cause species to be reduced.
(4) Add reactions that are reduced, but only involve species that are not reduced by step (3). With this step the number of input parameters (degrees of freedom) for the optimisation in step (5) is increased (optional).
(5) Optimise the reduced mechanism with concentration profiles of step (1) using the method from Section 2.3.

Similar schemes have been applied before for the reduction of chemical kinetics (e.g. [20]), but with the methods of the linTM, this reduction can be performed with significantly lower numerical effort. It should be noted that this scheme is quickly and plainly reducing reactions and species, becoming a new, additional tool for the reduction of chemical kinetic models. For a more sophisticated reduction this method can be combined with established reduction analytics and methods like reaction flow analysis and lumping of reactions and species (e.g. [16, 17]). A validation of our method is shown by the reduction of the biogenic gas mechanism in Section 4.

2.5 *Modelling of shock tube and flow reactor data for the optimisation*

As target data for the chemical kinetic model optimisation in Section 4, measured species profiles from OH(A) and CH(A) radical emission from ignition events in a shock tube [14] were selected. Depending on the evolution of the measured pressure profile of the experiment, the simulation was performed at constant pressure or using the measured pressure profile, assuming isentropic compression or expansion as proposed by Li et al. [23]. For the optimisation with the OH(A) and CH(A) emission profiles only the time domain of the characteristic points was considered because the concentration quantification of these experiments has high uncertainties. As shown in Figure 6, depending on the measured pressure profile different parts of the concentration time profiles were considered for optimisation: (a) for smooth pressure profiles during ignition the whole profile is considered; (b) for pressure profiles with a high pressure rise during ignition, only the concentration profile until the first peak of the underlying pressure profile was considered; (c) for pressure profiles with a strong pressure rise only the base characteristic point $\Pi_{j,20\%,\mathrm{s}}$ was considered. This strategy of limited utilisation of concentration profiles was chosen due to gas kinetic effects after the ignition blast wave, making

homogeneous simulations inapplicable [24].

As additional target data for the optimisation in Section 4, measured species profiles from a flow reactor [15] were selected. To simulate the species temperature profiles from flow reactors in Figure 7(a), each species result at a certain temperature is the result of a single homogeneous simulation of species time profiles in Figure 7(b) with a corresponding temperature time profile [15]. Since the measurement from the flow reactor is the single point of the simulation—here at points T_1, T_2 and T_3—the application of characteristic points is challenging. To apply characteristic points, the corresponding temperature time profiles for the simulation from [15], which would end at the temperature points in Figure 7(b), are extended at the end with the temperature held constant. Consequently, characteristic points can be set for reactants and products because the end point of their concentration profiles is well defined by the thermodynamic equilibrium. Figure 7 demonstrates that the selection of characteristic points is limited for intermediate species because the maximum—needed for characteristic point definition—of the species time profile is mostly unknown. In the experiment only the points T_1, T_2 and T_3 in Figure 7(b) can be measured. The complete evolution of the experimental species profile over the time is unknown for each experiment in Figure 7(b). For the measurement of a decreasing intermediate in the species temperature profile at point T_3, the actual maximum of the species time profile is unknown because the maximum is inside the flow reactor and cannot be measured. For an increasing intermediate at point T_1 the theoretical maximum cannot be measured because it would be after the flow reactor outlet. For intermediate species only the species maximum of the species temperature profile (a) at point T_2 can be utilised because it is approximately the maximum in the species time profile (b) as well.

3. Validation

The newly developed methods were numerically implemented in python and coupled with Cantera [18]. In principle, the presented methods can be easily coupled with any numerical combustion solver because only pre- and post-processing routines are needed. There is no need for adaptations of the solver itself. In the validation process of the optimisation method, the global sensitivity was investigated. For the validation, concentration time profiles of OH(A) and CH(A) radicals were simulated with an original chemical kinetic model to imitate 120 experiments of hydrogen and syngas ignition. Then, the original reaction model was randomly changed and subsequently optimised with the imitated experimental data. The original chemical kinetic model was derived from the GRI 3.0 model [25] by adding OH(A) and CH(A) subschemes from [26, 27]. The parameter boundaries were set to values from literature [27–29]. 137 input parameters τ_i of reactions with high global sensitivity coefficients S_r were optimised within their 3σ confidence intervals.

The validation was done in two parts. In the first part, no experimental error was added to the imitated experimental data, to check the overall performance of the optimisation method. In the second part of the validation, a realistic experimental error was added to the imitated experimental data, to check the capability of the method for application at realistic conditions. Furthermore, in the second part global sensitivity is evaluated. The rapid reduction scheme is validated by the results in Section 4.

As an indicator for the average distance between the predicted rate coefficients and the ones of the original model Θ in a defined temperature range, the root mean

square (rms) of this distance is evaluated:

$$\Delta_\Theta \lg(k(T))_{\mathrm{rms}} = \sqrt{\frac{\int_{T_1}^{T_2} \Delta_\Theta \lg^2(k(T))\, dT}{T_2 - T_1}} = \sqrt{\frac{\int_{T_1}^{T_2} \lg^2(k(T)/k_\Theta(T))\, dT}{T_2 - T_1}}. \quad (14)$$

Thus, $\Delta_\Theta \lg(k(T))_{\mathrm{rms}}$ is used to evaluate the quality of the predicted rate coefficient. To cover the main temperature range of the characteristic points, the temperatures T_1 and T_2 were set to 1000 K and 2000 K. The results of Equation (14) are compared to the possible maximum of the rms $\Delta_\Theta \lg(k_+(T))_{\mathrm{rms}}$, which refers to the rms of the boundaries of the confidence interval. It should be noted that the temperature range of the boundaries given in literature, e.g. in [28], might be out of the evaluated temperature range of 1000 K and 2000 K. That causes $\Delta_\Theta \lg(k_+(T))$ to be higher outside the given temperature range of literature values and inside the evaluated temperature range, leading to a relatively high $\Delta_\Theta \lg(k_+(T))_{\mathrm{rms}}$, which can be seen in Tables 1 and 2.

3.1 *Validation with imitated experimental data without error*

For the validation on experimental data without error only data for the OH(A) concentrations was considered because the data was sufficient for optimisation of the fitness F and the input parameters. For the 120 OH(A) concentration profiles 573 characteristic points were defined. Since the optimisation on real data is supposed to be done with shock tube data with high uncertainties of the concentration, only time related distances of characteristic points $d_{j,t}$ were considered. Additionally, the optimisation method presented in Section 2.3 is compared to a real coded genetic algorithm (GA), with the same definition of the fitness F. Regarding the GA, the population of newly formed parameter sets, created by cross over and random mutation, was set to 137. With this number of newly created parameter sets the numerical effort of the iteration step GA is equalised to the one of the method of least squares (LS), which needs to evaluate the brute force sensitivities of the 137 input parameters. More details on genetic algorithms can be found in the literature (e.g. [12, 30]).

Figure 8 shows that the optimisation problem is solved by the GA and LS. The performance of the GA is satisfying because the average deviation of the optimised distances is 1.3% and the highest deviation of a single distance is 11%. The LS outperforms the GA in terms of speed and accuracy by far. For the LS, the average deviation of the optimised distances is 0.008% and the highest deviation of a single distance is 0.078%. After approximately 10 iterations the LS converged, meaning 1370 mechanisms (10 times 137 input parameters) needed to be evaluated by brute force analyses. This number is considerably smaller compared to optimisations with response surface methods. As an example, Varga et al. needed to evaluate at least 10 000 supporting points or mechanisms respectively for a response surface optimisation of 30 parameters of a hydrogen mechanism [11] and 20 000 supporting points for a similar optimisation of 54 parameters of a syngas mechanism [31]. Even though the extent of real experimental data used for the optimisations by Varga et al. [11, 31] is not fully comparable to this validation, the validation in the next section shows that increasing the number of experiments and adding an experimental error to the data, does not affect the convergence speed noticeably. Thus, revealing the potential of the LS with the gradient approximation method of the linTM, to reduce numerical costs of optimisation of chemical kinetics by at least one order of magnitude.

Table 1 shows that the rate coefficients can be predicted by the optimisation with LS with outstanding high accuracy, for optimisation on time related distances only. The rms values, indicating average distances between predicted rate coefficients and the ones of the original model Θ, are remarkably small compared to the maximum rms of $\Delta_\Theta \lg(k_+(T))$. Such an accuracy could not be achieved by the GA. But, real experiments have an experimental error, which has a high influence on predicting the rate coefficients. This will be considered in the next section.

3.2 *Validation with imitated experimental data with error*

We assumed a maximum standard deviation of the error of the time related distances of 0.15 for shock tube experiments, mainly caused by the determination of the initial temperature [32, 33]. The generation of the erroneous experimental target data was performed by adding a Gaussian distributed temperature error to the original initial temperatures of the imitated experiments with a maximum standard deviation of 5 K. For the applied optimisation data set, this process caused a maximum distance error of 0.35 between the target data and the simulation data with the original initial temperatures and the original model Θ. For this validation, CH(A) concentrations were considered additionally. For the same reasons as in Section 3.1, only time related distances of characteristic points $d_{j,t}$ were considered. For the OH(A) and CH(A) profiles, 935 characteristic points were defined. To check the robustness of the optimisation method, 10 different input parameter sets for multiple optimisations were obtained with a Monte Carlo method, forming 10 initial chemical kinetic models.

Figure 9 shows the convergence of the fitness minimisation of the different initial chemical kinetic models. For the initial models, different solutions are found. As shown in Figure 10, the 10 different solutions found for different $k_r(T)$ can differ significantly. Compared to that, the resulting fitnesses of the multiple solutions in Figure 9 are almost equal to the fitness F_Θ of the original chemical kinetic model, which therefore can be utilised to evaluate the average error of experimental sets. The variety of solution is also displayed in Table 2 by the exemplary optimisation results of the rms of two different initial models. The accuracy of the predicted rate coefficients indicated by the rms differs a lot for the different solutions of parameter sets. But, by calculating the average rate coefficients $\bar{k}_r$ of the 10 solutions of k_r with:

$$\ln(\bar{k}_r(T)) = \sum_{m=1}^{10} \frac{\ln(k_{r,m}(T))}{10}, \tag{15}$$

the rate coefficients can be predicted with high accuracy. The rms values of $\bar{k}_r$ in Table 2 indicate low average distances between the original model Θ and the predicted model compared to their maximum possible rms value. Examples of $\bar{k}_r$ are also displayed in Figure 10.

The variance of the different solutions might be caused by the limited domain of experimental boundary conditions of the imitated shock tube experiments. This problem might be solved by adding a variety of different experiments, e.g. data from flow reactors or rapid compression machines, which would broaden the experimental boundary conditions by means of temperature, pressure and composition ranges. Furthermore, a high variance renders the interpretation of the uncertainty analysis more difficult. For example, the variance of the rate coefficients of each single solution can differ a lot for different temperatures, as seen for the several

solutions of reaction $H+O_2+AR \rightleftharpoons HO_2+AR$ in Figure 10. At 2000 K the deviation of the solutions of the rate coefficients is very high, whereas the solution of the average rate coefficient $\bar{k}_r$ is very close to the rate coefficient of the original model Θ. Contrary, at 1100 K, the deviation of the solutions of the rate coefficients is smaller than the distance between $\bar{k}_r$ and the rate coefficient of the original model Θ. Consequently, the variance of the different solutions can be misleading for the uncertainty analysis.

From the brute force sensitivity matrix $\mathbf{A}$ of the optimisation process of the 10 initial models the global sensitivity S_r is calculated at each iteration step and the results are summarised in Figure 11. The average and standard deviation of the calculated S_r during the optimisation process of a few key reactions are summarised in Figure 12. For most sensitive reactions like R1 and R2 the global sensitivity is very robust with low variance during the optimisation process. As an exception R3 in Figure 11 was less robust. A reason for the high deviation of S_r of R3 might be a too conservative assumption of the boundaries of the confidence interval $\Delta \lg (k_{r,+}(T)) = 0.5$, for which the fundamental assumption of constant gradients in the linTM does not apply sufficiently. Nevertheless, these reactions can be identified by this sensitivity analysis of the iterations, being an indicator for reactions that might not be predicted well by optimisation with indirect experiments. But, this method identifies the reactions that need to be investigated in more detail by other methods like quantum chemical calculations or if possible by direct measurements.

Even though this global sensitivity analysis was constructed for the optimisation within the linTM, it shows a great potential for a new efficient global sensitivity analysis. As an example, Davis et al. [5] had to evaluate 250 000 sampling points or chemical kinetic models respectively, for a Monte Carlo based global sensitivity analysis of a chemical kinetic model for hydrogen oxygen combustion with 25 rate coefficients. Compared to that, in the linTM only one kinetic model is needed per input parameter for its global sensitivity analysis. Considering reactions with global sensitivity coefficients S_r that have a high variance, a hybrid approach of a relatively small Monte Carlo simulation with the subsequent application of the sensitivity analysis of whole species profiles of the linTM, offers a convenient compromise between low numerical costs and sufficient global analysis.

4. Results and discussion

For a first application of the linTM, a chemical kinetic model is optimised on a small data set of methane combustion. Additionally, the derived model is reduced for the combustion of a biogenic gas mixture with the new method of rapid reduction proposed in Section 2.4.

4.1 *Experimental and numerical setup*

The experimental target set for the optimisation consists of data from a shock tube [14], a flow reactor [15] and laminar flame speeds [13]. The shock tube experiments are data from photon emission of excited OH(A) and CH(A) radicals from ignition delay time measurements. The shock tube experiments are listed in Table 3, for which the gas mixture of methane and oxygen was diluted 1/17.4 with argon. Temperature and pressure are given for the state of the initialised test gas after the reflected shock wave. From the flow reactor experiments concentration profiles of CH_4, H_2, O_2, CO, CO_2, H_2O, C_2H_2, C_2H_4, and C_2H_6 from the reaction of methane with oxygen were selected as target data for the optimisation process.

The flow reactor experiments are listed in Table 3, for which the gas mixture of methane and oxygen was diluted 1/100.0 with argon. For the laminar flame speed profiles methane air flames with the initial temperature of 298 K and pressures of 1 atm, 2 atm and 4 atm were selected as target data. Additionally, experimental results of flame speeds of a biogenic gas mixture [14] were used for validation of the optimisation results. For this experiment only flame speeds of the stretched flame were measured, which are referred to laminar burning velocities u_l. Due to stretch, mass and heat transfer in a flame are influenced, causing a change in the speed of the flame front compared to the laminar flame speed u_l^0 of the unstretched flame [34]. Nevertheless, the maximum error between u_l and u_l^0 of this biogenic flame was estimated to be below 10% [14]. For more details on the experimental setup of each experiment see [13–15]. From the experimental data, a total of 161 characteristic points, as explained in Sections 2.1.3 and 2.5, were defined for the optimisation.

The initial chemical kinetic model for optimisation was derived from the in-house model DLR-RG [35] by adding the OH(A) and CH(A) subschemes from [26, 27], which was also done in prior work (e.g. [14]). The initial model consists of 65 species and 389 reactions. Reactions with a global sensitivity coefficient S_r bigger than 1% of maximum S_r were set to values and parameter boundaries from literature [27–29], except for the collision efficiencies and fall-off coefficients, which were not optimised and kept from the more current base models. By doing so, the rate coefficients are not exactly adopted, but since these reactions are part of the optimisation, the error of the initial model can be neglected. From the selected reactions a total of 88 model input parameters were optimised within their 3σ confidence intervals. From a Monte Carlo simulation with 100 variations of the initial model, 4 additional initial chemical kinetic models with the lowest fitness F were selected for the optimisation, for the evaluation of the results. Figure 13 sums up the average $\bar{S}_r$ and the standard deviation of the global sensitivities of the reactions S_r during the optimisation process of the 5 different initial models.

4.2 *Optimisation and rapid reduction*

With the optimisation of the chemical kinetic models on the relatively small experimental set, different solutions with similar fitness F or predictability of experiments were derived, as already seen in the validation process in Section 3. The average distance of the characteristic points between simulation and experiment was reduced to approximately 7%. Exemplary the numerical predictions by one optimised chemical kinetic model of the target flame speed profiles are shown in Figure 14, verifying the optimisation method of flame speed profiles, as suggested in Section 2.1.3. No significant differences were noticed between the corresponding laminar flame speed predictions of the other 4 optimised models. For the shock tube data, the standard deviation of the distances between experimental and simulation results on the time axis was 6% after the optimisation. This value is considerably small compared to the typical standard deviation of 15% of the experimental error of these distances (see Section 3.2). The reason of this discrepancy can be an overestimation of the experimental error or the rather small statistical data set of the selected experiments, which can cause a high statistical error.

Nevertheless, as shown in Figure 15 the predicted maximum laminar flame speeds of most optimised models for the biogenic gas mixture, that were not target data of the optimisation, are in better agreement to the experimental results [14] than the predicted laminar flame speeds of the established chemical kinetic models GRI 3.0 [25] and DLR-RG [35]. The shift between measurements and predictions

in the direction of φ might be caused by differences between the stretched experimental flame and the unstretched simulated flame, as discussed above. The additional characteristic point number 162 $\Gamma_{162,100\%}$ (see Section 2.1.3), was analysed by sensitivity analysis to investigate the maximum flame speed of this flame speed profile. As seen in Figure 16 the most sensitive reaction is R24, for which only the low pressure rate coefficient $k_{24,\mathrm{low}}$ is sensitive for the investigated experiments. The different optimisation results for R24 in Figure 17 thereby indicate that the evaluation by Baulch et al. [28], which was done for temperatures below 1000 K, might overestimate the rate coefficient at higher temperatures, that might cause the high discrepancies between measurements and predictions of established models. However, an accurate estimation of the rate coefficient with the optimisation with this relatively small experimental set is not possible, especially because Figure 17 shows a high variance for the different predictions of the rate coefficient of reaction R46, which is the most sensitive reaction of the overall optimisation (Figure 13). Therefore, the correlations between the results of rate coefficients [11], might have a high influence on the results of R24. For a more comprehensive analysis and determination of the flame speeds of the biogenic gas mixture, rate coefficients of reactions R24 and R46, and of the complete chemical kinetic model, a larger experimental data set is needed for the optimisation, which is part of our ongoing work.

For the biogenic gas mixture a reduced model was derived by the rapid reduction scheme. The detailed base chemical kinetic model was one of the optimised models (65 species, 389 reactions), marked with triangles in Figure 15. For step (1) in the rapid reduction scheme (see Section 2.4) target data was created by homogeneous simulations of the ignition of the biogenic gas at constant pressure with the detailed model. Start temperatures for the simulations were chosen to be 1300 K, 1600 K, 2000 K, and 2400 K at 3 bar and equivalence ratios φ of 0.9, 1.3 and 1.7. For the 12 resulting simulations the mole fraction profiles of CH_4, H_2, O_2, CO, CO_2, H_2O, H, O, OH, CH_3, CH_2O, and N_2 were selected and characteristic points defined. The reduction was performed for a total of 629 resulting characteristic points, serving as target data. The reduced model consists of 16 species (including N_2 as an inert species) and 51 reactions. The average distance of the characteristic points of the optimised, reduced model is 0.5%. The laminar flame speeds predicted by the reduced model are in very good agreement with the detailed model and the error between the numerical results in Figure 15 is below 10%. If a higher accuracy for flame speed predictions was needed, flame speed profiles could be utilised as additional target data for the post optimisation. Laminar flame speeds are mainly driven by the heat conduction caused by the temperature gradients. The temperature gradient is highly dependent on the reactions rates or chemical time scales respectively. Since the optimisation method targets the whole species profiles, the time scales of the reactants, products and intermediate production and consumption are given in good agreement by the optimised model. Furthermore, laminar flame speeds are influenced by diffusion and thermodiffusion, which are highly dependent on the quantitative concentrations of the species. Thus, the reduction optimisation step targets on same chemical time scales and concentrations as the detailed model, leading to similar heat conduction, diffusion and thermodiffusion, consequently, leading to similar laminar flame speeds. The computational time of the whole reduction process was approximately 10 minutes on 20 state of the art CPU of 2015. Thus, with this approach, chemical kinetic models can be quickly reduced with a high grade of automation, making this reduction method a suitable tool for a variety of users.

5. Conclusions

The extensive validation and application of the easy to implement methods of the linTM have revealed the capability of the new methods to contribute significantly to numerical chemical kinetics. The validation has demonstrated the potential of reducing numerical costs of model optimisation on experimental data with the gradient approximation method of linTM by at least one order of magnitude compared to established methods. The successful optimisation on whole species profiles confirms the applicability of optimisation methods for accurate predictions of rate coefficients. Furthermore, the linTM offers new possibilities of analysis of chemical kinetic models with its efficient, robust and quantitative global sensitivity coefficient. In addition, the combination of these efficient analysis and optimisation methods allows the creation of the quick and easy to automatise method of rapid reduction of chemical kinetic models.

The first application of this optimisation on real experimental data shows promising results. With the optimisation, experiments from shock tubes, flow reactors and laminar flame speeds were incorporated with the linTM. A detailed chemical kinetic model for the combustion of methane was optimised, capable of reproducing experimental results more accurately compared to established models. The analysis and validation of the model indicate that the rate coefficient of the low pressure regime of reaction $H+CH_3(+M)\rightleftharpoons CH_4(+M)$ needs to be investigated in more detail for temperatures above 1000 K, especially to reproduce combustion parameters, such as laminar flame speeds of mixtures of H_2, CO and CH_4 or biogenic gases respectively. Furthermore, an efficient chemical kinetic model was derived by the new rapid reduction scheme, utilising the linTM, serving as a new, additional reduction tool. The relatively small number of experiments used for optimisation limited a more extensive analysis of experiments and the detailed chemical kinetic model. Thus, the optimisation of detailed chemical kinetic models with more experiments and therefore more control points is part of ongoing work.

On the whole, chemical kinetics can support achieving social and economic challenges in energy conversion by combustion applications. Thus, new detailed and reduced chemical kinetic models derived from the linTM can help in the numerical design and the optimisation of combustion applications, assuring their reliable operation at low emission levels.

Acknowledgement

The support by the Helmholtz-Gemeinschaft within the project DLR@Uni is thankfully acknowledged.

References

[1] T. Methling, M. Braun-Unkhoff, and U. Riedel, *A chemical-kinetic investigation of combustion properties of alternative fuels – A step towards more efficient power generation*, in *Proceedings of the ASME Turbo Expo: Turbine Technical Conference and Exposition, 2013*, GT2013-94994, American Society of Mechanical Engineers, San Antonio, USA, 2013.

[2] T. Methling, N. Armbrust, T. Haitz, M. Speidel, N. Poboss, M. Braun-Unkhoff, H. Dieter, B. Kempter-Regel, G. Kraaij, U. Schliessmann, Y. Sterr, A. Wörner, T. Hirth, U. Riedel, and G. Scheffknecht, *Power generation based on biomass by combined fermentation and gasification – A new concept derived from experiments and modelling*, Bioresour. Technol. 169 (2014), pp. 510–517.

[3] T. Methling, T. Kathrotia, M. Braun-Unkhoff, U. Riedel, J. Kiecherer, and M. Olzmann, *The pyrolysis of ethanol: Kinetic modeling of shock tube experiments*, in *Proceedings of the European Combustion Meeting - 2015*, P1-51, Budapest, Hungary, 2015.

[4] J. Warnatz, U. Maas, and R. Dibble, *Combustion: Physical and Chemical Fundamentals, Modeling and Simulation, Experiments, Pollutant Formation*, 4th ed., Springer Berlin Heidelberg, 2006.

[5] M.J. Davis, R.T. Skodje, and A.S. Tomlin, *Global sensitivity analysis of chemical-kinetic reaction mechanisms: construction and deconstruction of the probability density function*, The Journal of Physical Chemistry A 115 (2011), pp. 1556–1578.

[6] T. Turányi and A.S. Tomlin, *Analysis of Kinetic Reaction Mechanisms*, Springer Berlin Heidelberg, 2014.

[7] X. You, H. Wang, E. Goos, C.J. Sung, and S.J. Klippenstein, *Reaction kinetics of CO + HO_2 → products: ab initio transition state theory study with master equation modeling*, J. Phys. Chem. A 111 (2007), pp. 4031–4042.

[8] I.G. Zsély, T. Varga, T. Nagy, M. Cserháti, T. Turányi, S. Peukert, M. Braun-Unkhoff, C. Naumann, and U. Riedel, *Determination of rate parameters of cyclohexane and 1-hexene decomposition reactions*, Energy 43 (2012), pp. 85–93.

[9] S.G. Davis, A.V. Joshi, H. Wang, and F. Egolfopoulos, *An optimized kinetic model of H_2/CO combustion*, Proceedings of the Combustion Institute 30 (2005), pp. 1283–1292.

[10] X. You, T. Russi, A. Packard, and M. Frenklach, *Optimization of combustion kinetic models on a feasible set*, Proceedings of the Combustion Institute 33 (2011), pp. 509–516.

[11] T. Varga, T. Nagy, C. Olm, I.G. Zsély, R. Pálvölgyi, É. Valkó, G. Vincze, M. Cserháti, H. Curran, and T. Turányi, *Optimization of a hydrogen combustion mechanism using both direct and indirect measurements*, Proceedings of the Combustion Institute 35 (2015), pp. 589–596.

[12] F. Perini, J.L. Brakora, R.D. Reitz, and G. Cantore, *Development of reduced and optimized reaction mechanisms based on genetic algorithms and element flux analysis*, Combustion and Flame 159 (2012), pp. 103–119.

[13] O. Park, P.S. Veloo, N. Liu, and F.N. Egolfopoulos, *Combustion characteristics of alternative gaseous fuels*, Proceedings of the Combustion Institute 33 (2011), pp. 887–894, Available at http://www.sciencedirect.com/science/article/pii/S1540748910002026.

[14] J. Herzler, J. Herbst, T. Kick, C. Naumann, M. Braun-Unkhoff, and U. Riedel, *Alternative fuels based on biomass: An investigation of combustion properties of product gases*, Journal of Engineering for Gas Turbines and Power 135 (2013), p. 031401.

[15] P. Oßwald and M. Köhler, *An atmospheric pressure high-temperature laminar flow reactor for investigation of combustion and related gas phase reaction systems*, Review of Scientific Instruments 86 (2015), 105109.

[16] A.S. Tomlin, T. Turányi, and M.J. Pilling, *Mathematical tools for the construction, investigation and reduction of combustion mechanisms*, Comprehensive Chemical Kinetics 35 (1997), pp. 293–437.

[17] P. Pepiot-Desjardins and H. Pitsch, *An automatic chemical lumping method for the reduction of large chemical kinetic mechanisms*, Combustion Theory and Modelling 12 (2008), pp. 1089–1108.

[18] D.G. Goodwin, H.K. Moffat, and R.L. Speth, *Cantera: An object-oriented software toolkit for chemical kinetics, thermodynamics, and transport processes*, http://www.cantera.org (2015), version 2.2.0.

[19] N. Jaouen, P. Domingo, and L. Vervisch, *Using genetic algorithm for automated optimization of reduced chemical schemes*, in *Proceedings of the European Combustion Meeting - 2015*, Budapest, Hungary, 2015.

[20] W. Polifke, W. Geng, and K. Döbbeling, *Optimization of rate coefficients for simplified reaction mechanisms with genetic algorithms*, Combustion and Flame 113 (1998), pp. 119–134.

[21] Z. Huang, Y. Zhang, K. Zeng, B. Liu, Q. Wang, and D. Jiang, *Measurements of laminar burning velocities for natural gas-hydrogen-air mixtures*, Combustion and Flame 146 (2006), pp. 302 – 311.

[22] S. Liao, D. Jiang, and Q. Cheng, *Determination of laminar burning velocities for natural gas*, Fuel 83 (2004), pp. 1247–1250.

[23] H. Li, Z.C. Owens, D.F. Davidson, and R.K. Hanson, *A simple reactive gasdynamic model for the computation of gas temperature and species concentrations behind reflected shock waves*, Int. J. Chem. Kinet. 40 (2008), pp. 189–198.

[24] K.P. Grogan and M. Ihme, *Weak and strong ignition of hydrogen/oxygen mixtures in shock-tube systems*, Proceedings of the Combustion Institute 35 (2015), pp. 2181 – 2189, Available at http://www.sciencedirect.com/science/article/pii/S1540748914003848.

[25] G.P. Smith, D.M. Golden, M. Frenklach, N.W. Moriarty, B. Eiteneer, M. Goldenberg, C.T. Bowman, R.K. Hanson, S. Song, W.C. Gardiner Jr., V.V. Lissianski, and Z. Qin, *GRI 3.0 mechanism*, http://www.me.berkeley.edu/gri_mech/ (1999), accessed: 2015-11-01.

[26] T. Kathrotia, U. Riedel, and J. Warnatz, *A numerical study on the relation of OH*, CH*, and C2* chemiluminescence and heat release in premixed methane flames*, in *Proceedings of the European Combustion Meeting - 2009*, P809002, Vienna, Austria, 2009.

[27] T. Kathrotia, M. Fikri, M. Bozkurt, M. Hartmann, U. Riedel, and C. Schulz, *Study of the H + O + M reaction forming OH*: Kinetics of OH* chemiluminescence in hydrogen combustion systems*, Combust. Flame 157 (2010), pp. 1261–1273.

[28] D.L. Baulch, C.T. Bowman, C.J. Cobos, R. Cox, T. Just, J.A. Kerr, M.J. Pilling, D. Stocker, J. Troe, W. Tsang, R.W. Walker, and J. Warnatz, *Evaluated kinetic data for combustion modeling: Supplement II*, J. Phys. Chem. Ref. Data 34 (2005), pp. 757–1397.

[29] Z. Hong, D.F. Davidson, and R.K. Hanson, *An improved H_2/O_2 mechanism based on recent shock tube/laser absorption measurements*, Combustion and Flame 158 (2011), pp. 633–644.

[30] L. Elliott, D. Ingham, A. Kyne, N. Mera, M. Pourkashanian, and C. Wilson, *Incorporation of physical bounds on rate parameters for reaction mechanism optimization using genetic algorithms*, Combustion Science and Technology 175 (2003), pp. 619–648.

[31] T. Varga, C. Olm, T. Nagy, I.G. Zsély, É. Valkó, R. Pálvölgyi, H.J. Curran, and T. Turányi, *Development of a joint hydrogen and syngas combustion mechanism based on an optimization approach*, International Journal of Chemical Kinetics (2016), pp. n/a–n/a, Available at http://dx.doi.org/10.1002/kin.21006.

[32] Z. Hong, R.D. Cook, D.F. Davidson, and R.K. Hanson, *A shock tube study of $OH + H_2O_2 \rightarrow H_2O + HO_2$ and $H_2O_2 + M \rightarrow 2OH + M$ using laser absorption of H_2O and OH*, The Journal of Physical Chemistry A 114 (2010), pp. 5718–5727.

[33] F. Rao, B. Li, P. Li, C. Zhang, and X. Li, *Shock-tube study of the ignition of gas-phase 1,3,5-trimethylbenzene in air*, Energy & Fuels 28 (2014), pp. 6707–6713.

[34] G. Markstein, *Non-steady combustion propagation*, The Macmillan Company, Pergamon Press, Oxford, 1964.

[35] M. Braun-Unkhoff, N. Slavinskaya, and M. Aigner, *A detailed and reduced reaction mechanism of biomass-based syngas fuels*, Journal of Engineering for Gas Turbines and Power 132 (2010), p. 091401.

Table 1. Accuracy of $k(T)$ of the optimised model compared to $k_\Theta(T)$

Reaction	S_r	$\Delta_\Theta \lg(k_r(T))_{\rm rms}$	$\Delta_\Theta \lg(k_{r,+}(T))_{\rm rms}$
$H+O_2+AR \rightleftharpoons HO_2+AR$	161.6	0.0012	0.18
$HO_2+CO \rightleftharpoons OH+CO_2$	79.0	0.0071	0.50
$H+O_2 \rightleftharpoons O+OH$	75.3	0.0009	0.05
$H+HO_2 \rightleftharpoons O_2+H_2$	61.5	0.0100	0.99
$H+O_2+M \rightleftharpoons HO_2+M$	60.5	0.0268	0.55
$H+H_2O_2 \rightleftharpoons HO_2+H_2$	56.7	0.0372	0.94
$O+H_2 \rightleftharpoons H+OH$	45.6	0.0050	0.20
$H+HO_2 \rightleftharpoons 2OH$	42.3	0.0162	0.49

Table 2. Accuracy of $k(T)$ of multiple optimised models compared to $k_\Theta(T)$

Reaction	S_r	$\Delta_\Theta \lg(k_{r,m}(T))_{\rm rms}$ $m=3$	$m=6$	$\cdots$	$\Delta_\Theta \lg(\bar{k}_r(T))_{\rm rms}$	$\Delta_\Theta \lg(k_{r,+}(T))_{\rm rms}$
$H+O_2+Ar \rightleftharpoons HO_2+Ar$	259.8	0.0286	0.0425		0.0428	0.18
$HO_2+CO \rightleftharpoons OH+CO_2$	171.1	0.3098	0.3026		0.2873	0.50
$H+HO_2 \rightleftharpoons O_2+H_2$	135.5	0.4494	0.3127		0.3840	0.99
$H+O_2 \rightleftharpoons O+OH$	126.8	0.0197	0.0147	$\cdots$	0.0199	0.05
$H+O_2+M \rightleftharpoons HO_2+M$	105.6	0.1222	0.2007		0.1110	0.55
$O+H_2 \rightleftharpoons H+OH$	76.0	0.0897	0.0651		0.0704	0.20
$H+HO_2 \rightleftharpoons 2OH$	70.2	0.0585	0.2142		0.1018	0.49
$OH+CO \rightleftharpoons H+CO_2$	70.0	0.0081	0.0202		0.0080	0.20

Table 3. List of experiments used for optimisation

Exp. no.	φ	T	p	Number of Π_j
Shock tube experiments [14]:				
1	1	1526.8 K	4 bar	8
2	1	1393.7 K	4 bar	6
3	1	1658.2 K	4 bar	8
4	1	1807.1 K	4 bar	8
5	1	1920.4 K	4 bar	8
6	1	2070.6 K	4 bar	11
7	1	1986.5 K	4 bar	11
8	1	1755.8 K	4 bar	10
9	1	1740.0 K	4 bar	12
10	1	1736.2 K	4 bar	12
11	1	1617.0 K	4 bar	10
12	1	1468.7 K	4 bar	4
Flow reactor experiments [15]:				
13	2	1349.0 K	1 bar	1
14	2	1312.0 K	1 bar	6
15	2	1310.0 K	1 bar	2
16	2	1307.0 K	1 bar	4
17	2	1302.0 K	1 bar	6
18	1	1251.5 K	1 bar	10
19	1	1248.5 K	1 bar	3
20	0.5	1203.5 K	1 bar	4
21	0.5	1200.0 K	1 bar	6

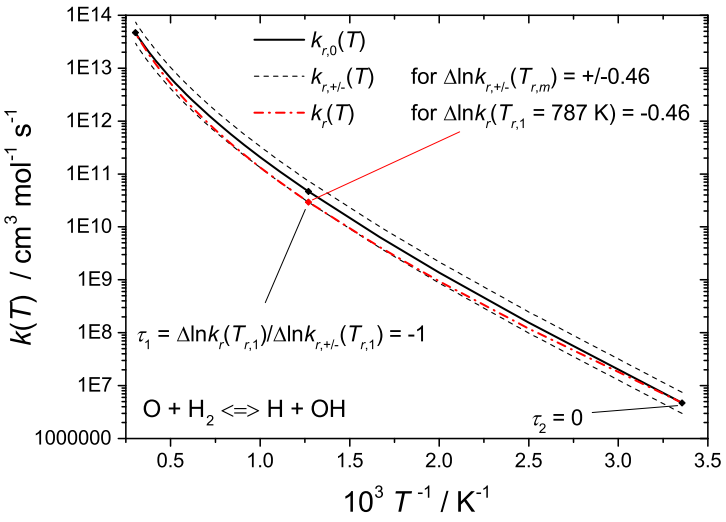

Figure 1. Exemplary rate coefficient k_r with the confidence interval $k_{r,+/-}$ and definition of τ_1 and τ_2

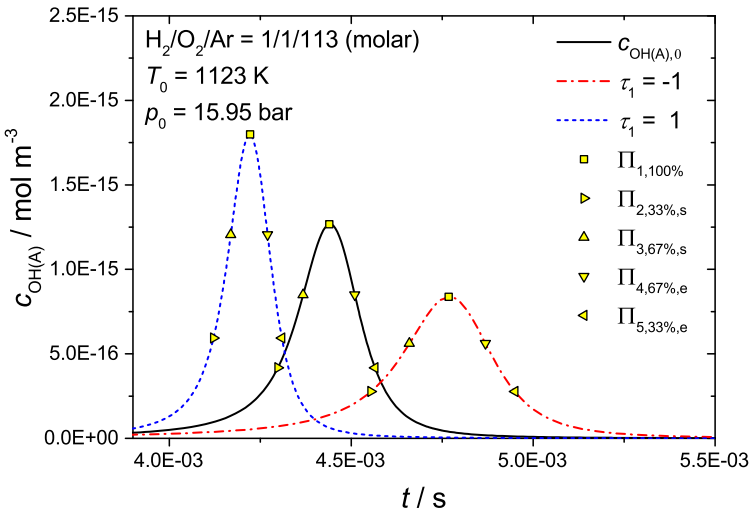

Figure 2. Dependency of the concentration time profile on parameter τ_1

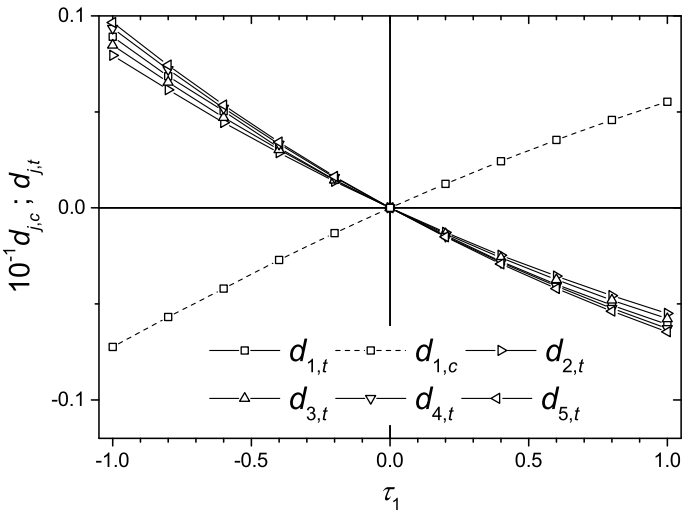

Figure 3. Dependency of distances $d_{j,t/c}$ on parameter τ_1

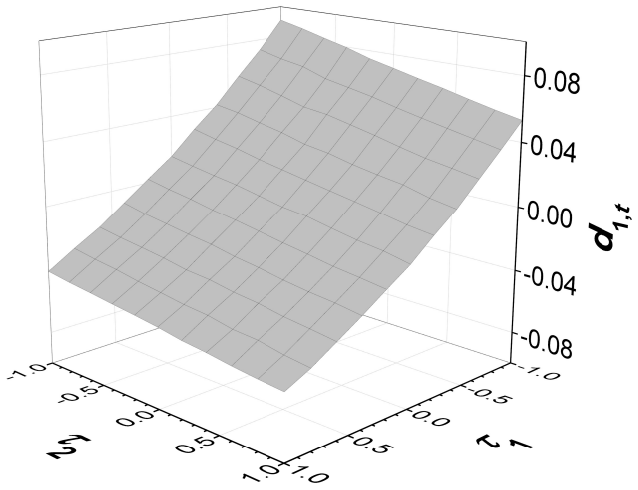

Figure 4. Dependency of distances $d_{1,t}$ on parameters τ_1 and τ_2

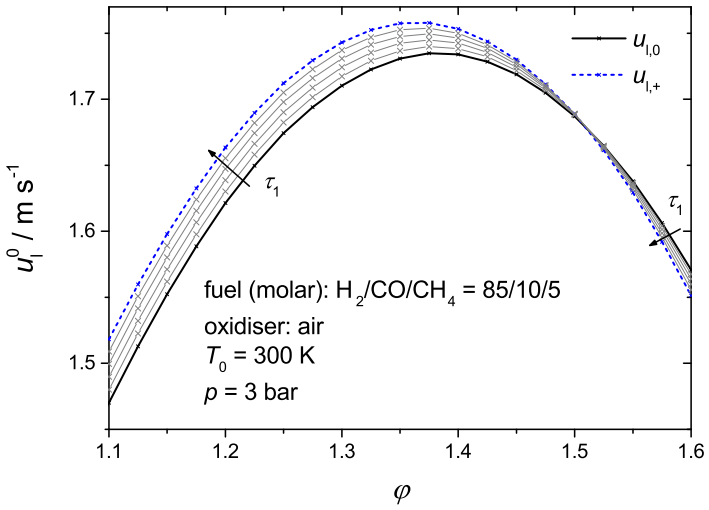

Figure 5. Dependency of laminar flame speed profile on parameter τ_1

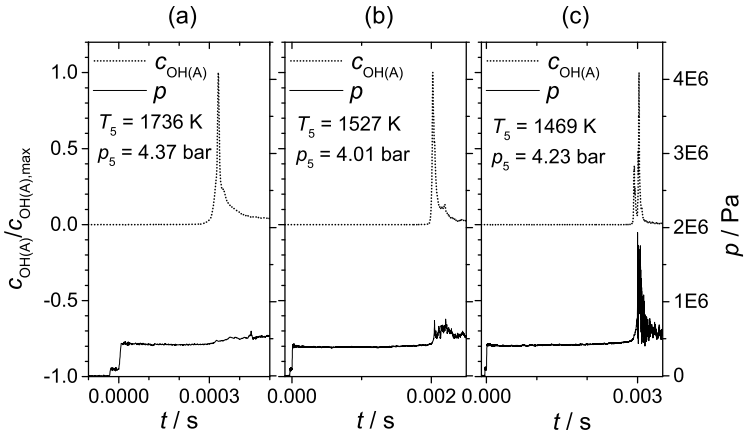

Figure 6. Measurement of filtered OH(A) and pressure profiles of shock tube experiments with equalised axis for concentration and pressure; molar composition ratio: $CH_4/O_2/Ar = 1/2/49$

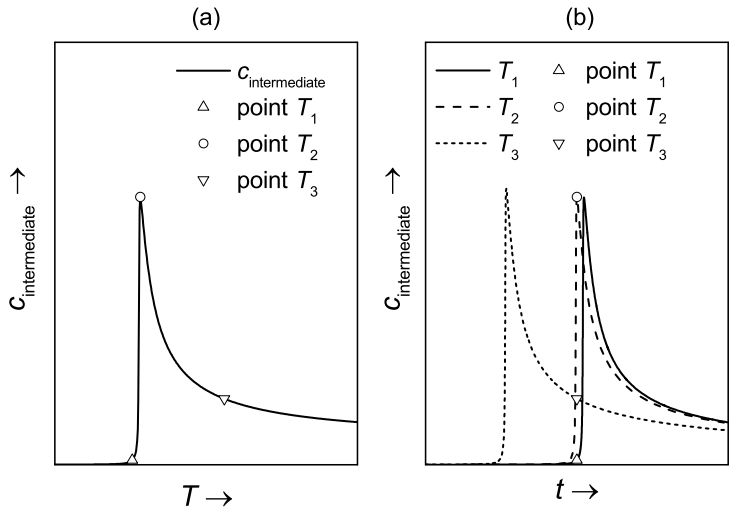

Figure 7. Schematic illustration of species temperature (a) and species time (b) profiles of flow reactor simulation

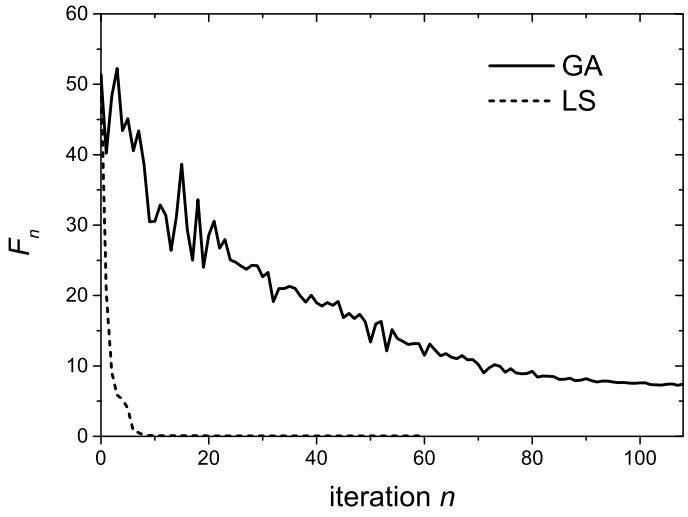

Figure 8. Optimisation progress for the validation with target data without error

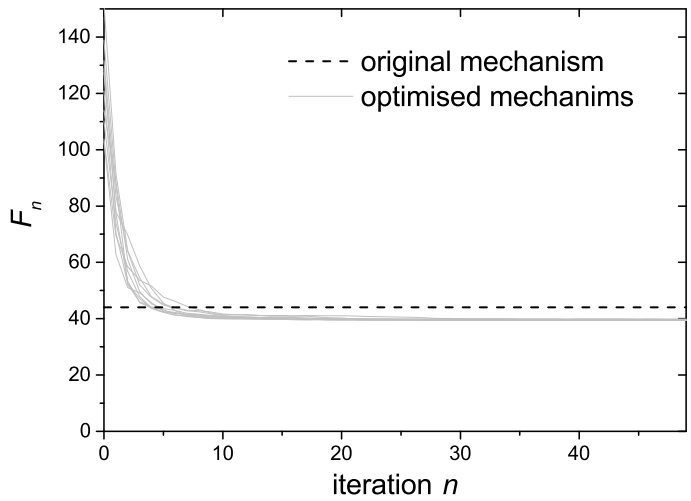

Figure 9. Optimisation progress for the validation of multiple initial solutions with target data with error

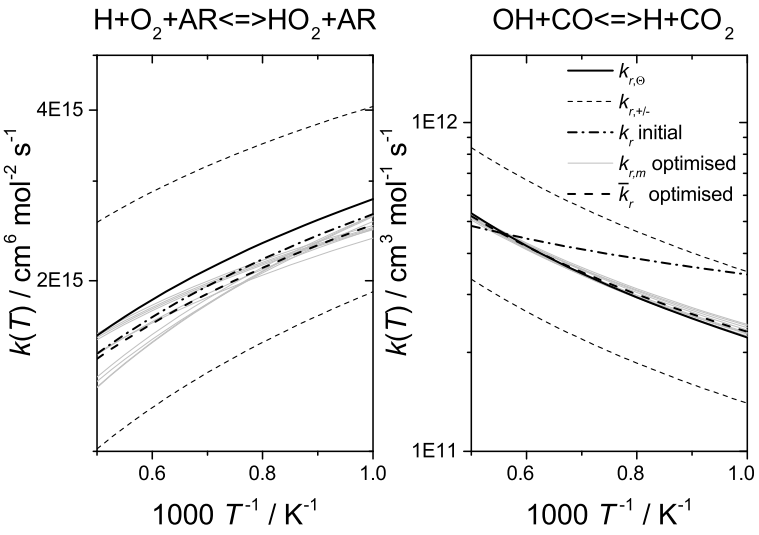

Figure 10. Deviation of different solutions of $k(T)$ to the original $k_\Theta(T)$

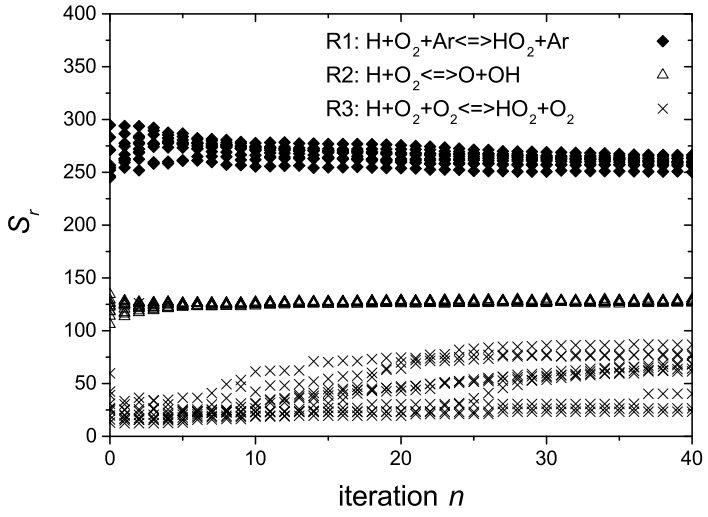

Figure 11. Evolution of S_r for different reactions during the optimisation progress

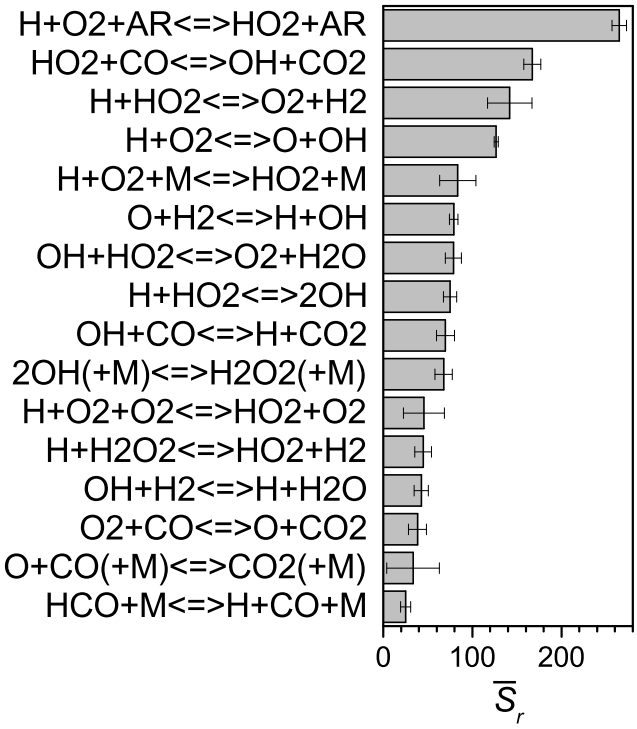

Figure 12. Average global sensitivity coefficients and their standard deviation during optimisation of the initial chemical kinetic models of the validation

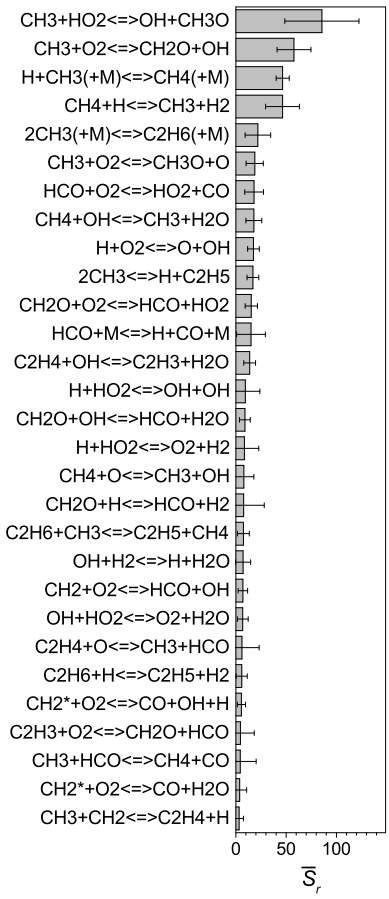

Figure 13. Average global sensitivity coefficients of all optimised rate coefficients and their standard deviation during optimisation of the initial chemical kinetic models

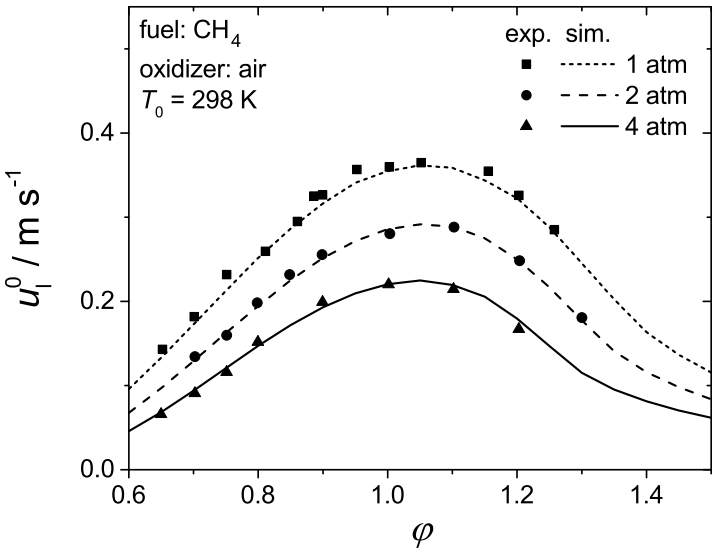

Figure 14. Laminar flame speed simulations of methane of an optimised chemical kinetic model compared to experiments from [13]

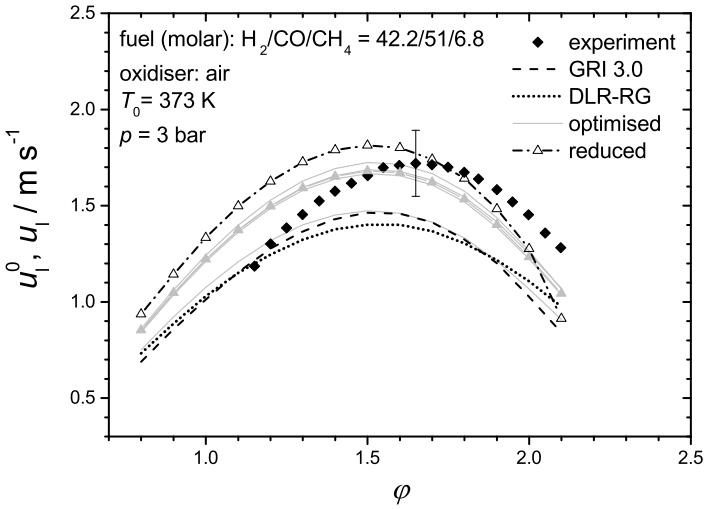

Figure 15. Numerical laminar flame speeds u_l^0 of a biogenic gas mixture compared to experimental laminar burning velocities u_l from [14]

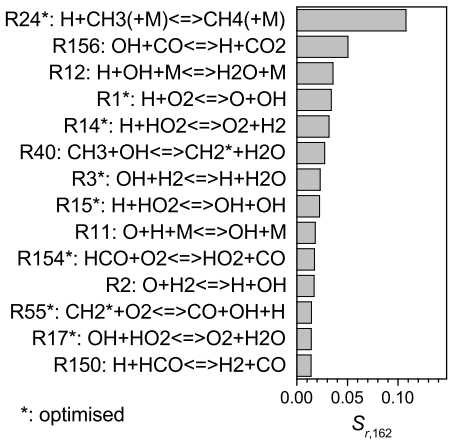

Figure 16. Sensitivity coefficient for the characteristic points of the maximum laminar flame speed

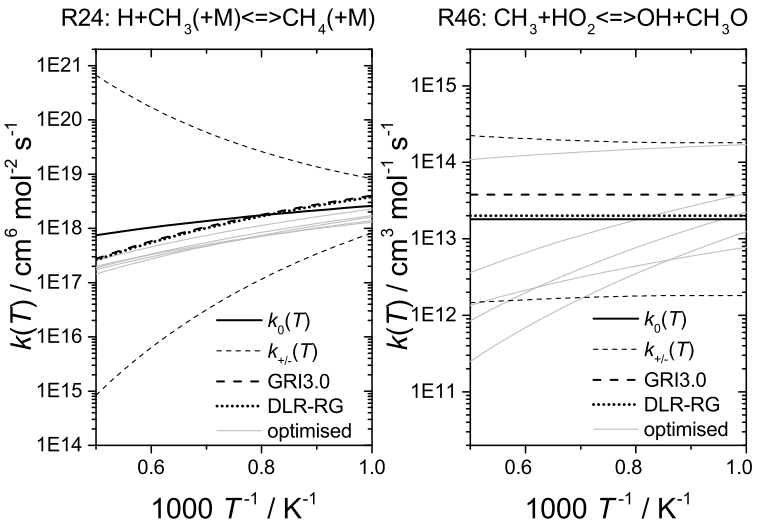

Figure 17. Optimisation results for $k_{24,\mathrm{low}}$ and k_{46} with their 2σ confidence intervals $k_{r,+/-}$